Cell Reports
Physical Science

Article

Enhancement of molecular conductance through a supramolecular five-molecule assembly

Graphical abstract

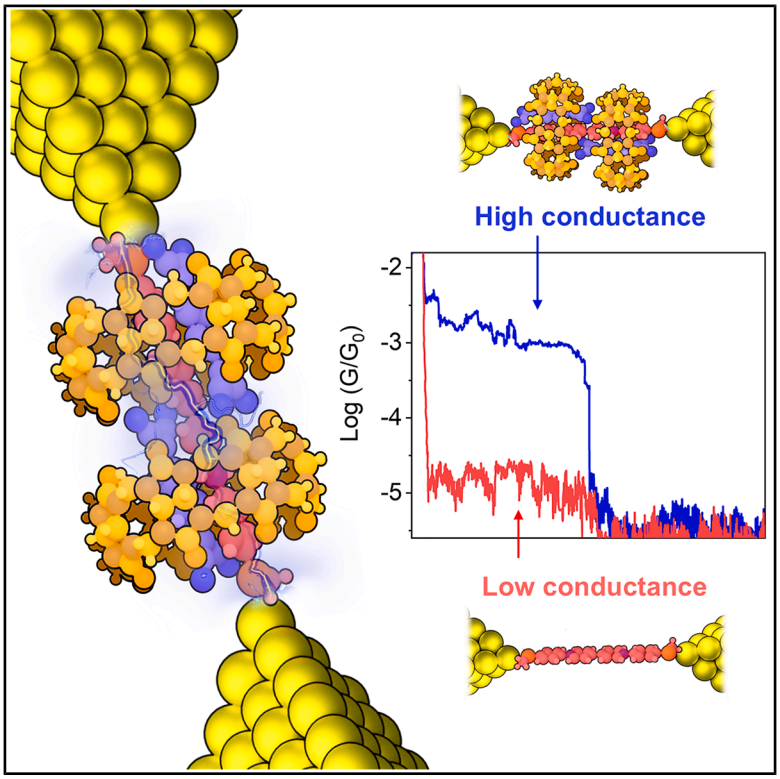

Highlights

- Fabrication of a stable supramolecular five-molecule host-guest assembly
- Single-molecule junctions of the assembly show a large enhancement of conductance
- Potential fabrication of molecular electronic components with reversible states

Authors

Enrique Escorihuela, Mauricio Regalado Aguilar, Biswajit Mondal, ..., Eliseo Ruiz, Albert C. Aragonès, Santiago Martín

Correspondence

eliseo.ruiz@qi.ub.edu (E.R.), acortijos@ub.edu (A.C.A.), smartins@unizar.es (S.M.)

In brief

Enrique Escorihuela et al. design a stable supramolecular five-molecule assembly by combining non-covalent and supramolecular interactions with a large enhancement of conductance. This result demonstrates a suitable strategy for the future fabrication of single-molecule electronic devices with reversible states, offering an alternative to the actual electronic device technologies.

Escorihuela et al., 2026, Cell Reports Physical Science 7, 103029
January 21, 2026
https://doi.org/10.1016/j.xcrp.2025.103029

CellPress

Cell Reports
Physical Science

CellPress
OPEN ACCESS

Article

Enhancement of molecular conductance through a supramolecular five-molecule assembly

Enrique Escorihuela,[1,2,8] Mauricio Regalado Aguilar,[3,4] Biswajit Mondal,[3,4] Sara Cuscó,[5] Pilar Romero,[1,6] Ross J. Davidson,[7] Pilar Cea,[1,2,8] Jordi Benet-Buchholz,[9] Eliseo Ruiz,[3,4,*] Albert C. Aragonès,[4,5,*] and Santiago Martín[1,2,8,10,*]

[1]Instituto de Nanociencia y Materiales de Aragón (INMA), CSIC-Universidad de Zaragoza, 50009 Zaragoza, Spain
[2]Departamento de Química Física, Facultad de Ciencias, Universidad de Zaragoza, 50009 Zaragoza, Spain
[3]Departament de Química Inorgànica i Orgànica, Universitat de Barcelona, 08028 Barcelona, Spain
[4]Institut de Química Teòrica i Computacional (IQTC), Universitat de Barcelona, 08028 Barcelona, Spain
[5]Departament de Ciència de Materials i Química Física, Universitat de Barcelona, 08028 Barcelona, Spain
[6]Departamento de Química Orgánica, Facultad de Ciencias, Universidad de Zaragoza, 50009 Zaragoza, Spain
[7]Department of Chemistry, Durham University, South Rd., Durham DH1 3LE, UK
[8]Laboratorio de Microscopias Avanzadas (LMA), Universidad de Zaragoza, 50018 Zaragoza, Spain
[9]Institute of Chemical Research of Catalonia (ICIQ), 43007 Tarragona, Spain
[10]Lead contact
*Correspondence: eliseo.ruiz@qi.ub.edu (E.R.), acortijos@ub.edu (A.C.A.), smartins@unizar.es (S.M.)
https://doi.org/10.1016/j.xcrp.2025.103029

SUMMARY

Achieving a comprehensive understanding and precise control of non-covalent interactions is crucial in molecular design and the development of functional molecular electronic devices, where supramolecular interactions enable the control of the local environment in molecular assemblies. Here, intermolecular interactions are used to create a complex supramolecular assembly by π stacking of 1,1′-bis(4-(methylthio)-phenyl)-[4,4′-bipyridine]-1,1′-diium chloride ($1[Cl]_2$) and tetracyanoquinodimethane radical anion ($TCNQ^{\cdot-}$), whose crystal structure is determined by an electron diffraction technique, showing the presence of stacked 1^{2+}-$2(TCNQ^{\cdot-})$ units. This solid dissolves in aqueous solutions of cucurbit[8]uril (CB[8]), which acts as the host, to form a supramolecular five-molecule $\{1^{2+}\text{-}2(TCNQ^{\cdot-})@2CB[8]\}$ assembly. Its transport properties result in a significant enhancement of conductance. Theoretical studies confirm the stability of the supramolecular assembly and corroborate the enhancement in conductance. These results present a simple and effective method for stabilizing and enhancing charge transport efficiency through a combination of non-covalent and supramolecular interactions, with significant implications for the development of future (opto)electronic devices.

INTRODUCTION

The application of molecules with appropriately designed chemical structures to perform one or more of the fundamental functions of the elements of an electronic circuit has given a major boost to the field of molecular electronics in recent decades.[1–4] In this context, electrode-molecule-electrode junctions have proven to be remarkably versatile research tools, providing the opportunity to directly measure the electrical properties of single molecules connected to two macroscopic electrodes under an applied bias voltage. Several strategies are available to fine-tune the electrical properties in single-molecule systems, exerting control over the molecular and electronic structure through external stimuli,[5–14] such as luminescent excitation,[6] solvent effects,[7] or electrochemical[8,15] or electrostatic[9] environmental gating; through supramolecular interactions[10,11,16]; or through intermolecular complexation.[10,12–14]

Supramolecular interactions, which encompass hydrogen bonds, van der Waals forces, ionic interactions, or π-π interactions, among others, play a crucial role in molecular recognition,[17,18] catalyst design,[19,20] or the assembly of larger molecular architectures,[21,22] as they largely govern the structure and properties of matter. In this sense, achieving a thorough understanding and precise control of these interactions is crucial for molecular design and the development of functional devices.[16,23] Some of these intermolecular contacts can involve orbital interactions, inducing partial or complete charge transfer between different species, leading to the emergence of new transport pathways through supramolecular structures that are based mainly on the existence of weak interactions along these transport pathways. These pathways can differ significantly from the original properties of the precursors.[10,13,24–27]

On the other hand, intermolecular complexation methodologies based on the formation of host-guest complexes have also been widely used in various applications, playing a crucial role in applications such as molecular recognition,[28,29] catalysis,[30] and drug encapsulation and delivery[31] or for designing supramolecular electronic devices.[12,16,32–34] In these supramolecular

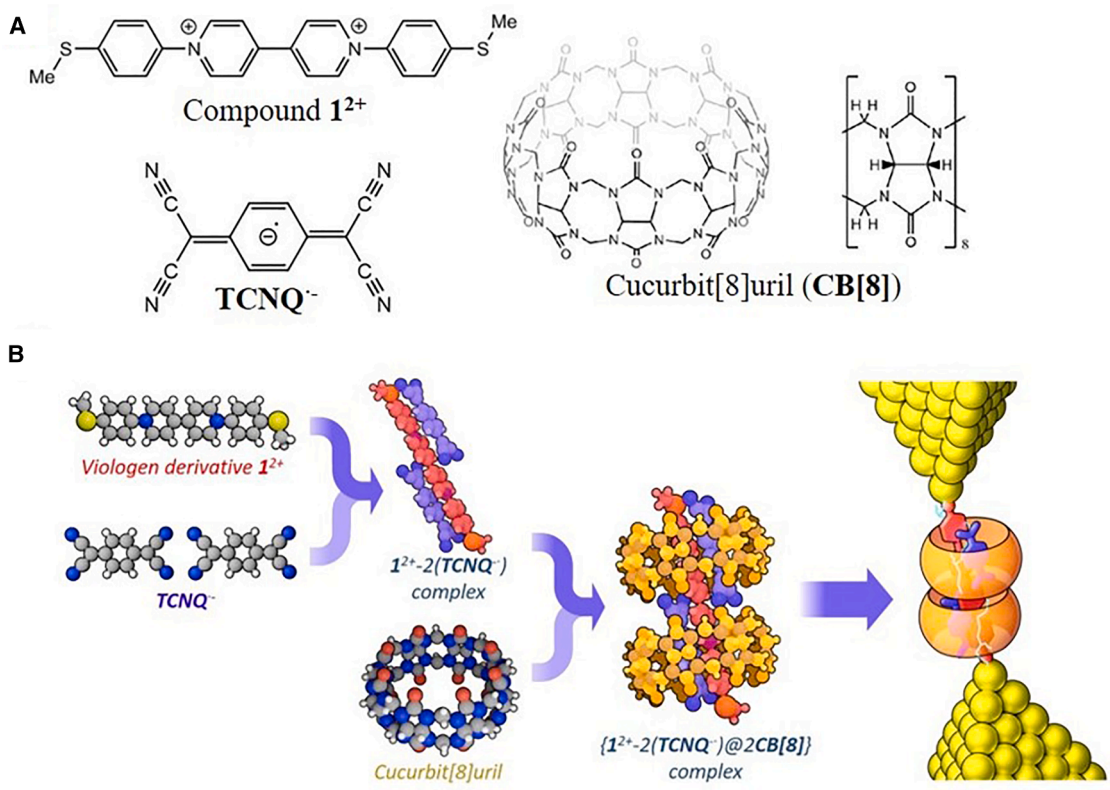

Scheme 1. Supramolecular five-molecule assembly design

(A) Structures of the viologen derivative, $\mathbf{1^{2+}}$, tetracyanoquinodimethane radical anion (**TCNQ**$^{\cdot-}$), and the host molecule cucurbit[8]uril, **CB[8]**.

(B) A scheme showing the strategy used to form the supramolecular five-molecule assembly, {$\mathbf{1^{2+}}$**-2(TCNQ**$^{\cdot-}$**)@2CB[8]**}, in aqueous solution and to determine its electrical properties.

structures, the host can modify the local environment of the guest, inducing changes in its properties, such as its solubility.[12] In addition, the host can restrict the conformation geometry and intramolecular mobility of the guest molecules, as well as avoid harmful intermolecular interactions with other species, thereby favoring the formation of a stable assembly in the single-molecule junction and reducing the spread of conductance values.[5,12,35]

Encouraged by the potential of the abovementioned supramolecular strategies, we present here the formation of a noncovalent assembly (Scheme 1) that significantly boosts its electronic properties up to $10^{-2.7}$ G_0 (2×10^{-3} G_0) by the combination of (1) the formation of a π-stacked three-molecule $\mathbf{1^{2+}}$**-2(TCNQ**$^{\cdot-}$**)** complex and (2) its insertion into a host cucurbituril molecule to form a supramolecular host-guest complex, which provides stability to the system in solution, enhancing its solubility and simultaneously shielding the complex against potential unwanted interactions with other species. To the best of our knowledge, only one similar case has been reported: a Pt^{II} metallocycle that, due to structural deformation caused by the inclusion of a fullerene within the cycle, exhibits an increase of one order of magnitude in conductance through the metallocycle.[36] Importantly, our system features an entirely different chemical composition and shows a greater increase in the conductance of two orders of magnitude driven by supramolecular interactions.

RESULTS AND DISCUSSIONS

π-stacked supramolecular formation

The π-stacked supramolecular system is formed by adding a 10^{-4} M aqueous solution of 1,1′-bis(4-(methylthio)-phenyl)-[4,4′-bipyridine]-1,1′-diium chloride (**1**[Cl_2]) directly over lithium tetracyanoquinodimethanate (LiTCNQ) powder in a 1:2 molar ratio, respectively. Figure 1 shows the UV-visible (UV-vis) spectra before and after this addition. Solutions of **1**[Cl_2] are yellow with two absorption bands centered at 260 and 400 nm. After the addition, the solution changes to a magenta color, where the spectrum displays bands attributed to both $\mathbf{1^{2+}}$ and **TCNQ**$^{\cdot-}$ radical anions, albeit with variations in intensity and position. Nevertheless, the most outstanding feature is the appearance of a new intense and broad band at 546 nm associated with a charge transfer band (Figures 1 and S1),[37] which evidences a notable interaction between $\mathbf{1^{2+}}$ and **TCNQ**$^{\cdot-}$. In addition, after 24 h, the formation of a dark precipitate is observed, caused by the low solubility of the formed neutral $\mathbf{1^{2+}}$**-2(TCNQ**$^{\cdot-}$**)** assemblies in water (Figure 1), as is also the case for similar complexes in polar and non-polar solvents.[24,38–41] The appearance of the precipitate, together with the practically colorlessness of the solution, indicates the complete reaction of almost all components, with no precursors remaining in the liquid phase, confirming the formation of the supramolecular π-stacked $\mathbf{1^{2+}}$**-2(TCNQ**$^{\cdot-}$**)** system.

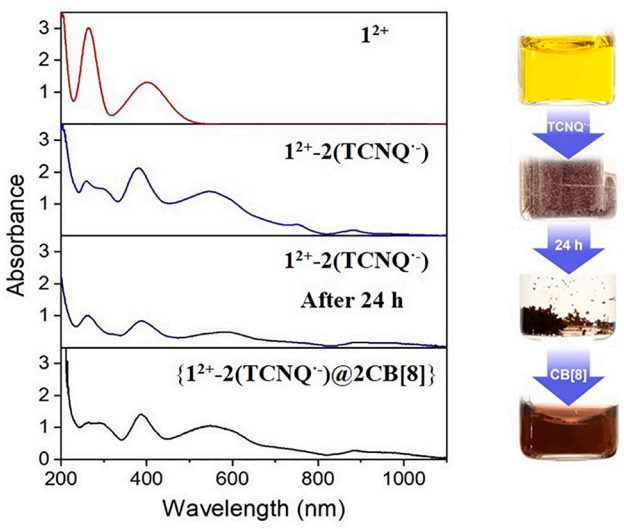

Figure 1. UV-vis spectroscopy characterization

UV-vis spectra for 10^{-4} M aqueous solutions of $\mathbf{1^{2+}}$ and $\mathbf{1^{2+}}$**-2(TCNQ$^{\cdot-}$)** in a 1:2 ratio and after 24 h and for {$\mathbf{1^{2+}}$**-2(TCNQ$^{\cdot-}$)@2CB[8]**}. See the supplemental information for a time-dependent density functional theory (TDDFT) analysis.

The absence of peaks in the ^{1}H-NMR spectrum for an aqueous solution of $\mathbf{1^{2+}}$**-2(TCNQ$^{\cdot-}$)** (Figure S7) suggests a paramagnetic behavior, that is, the presence of unpaired electrons in this system,[42] which is corroborated by electron paramagnetic resonance (EPR). The observation of only a broad signal in the EPR spectra for $\mathbf{1^{2+}}$**-2(TCNQ$^{\cdot-}$)**, both in powder and in an aqueous solution, with a *g* factor between 2.0081 and 2.0072 (Figure S8) confirms the presence of a radical moiety, in which other types of nuclear coupling are not distinguished, as has been observed for similar TCNQ complexes.[43] Additionally, the band at 2,188 cm^{-1} characteristic of the nitrile group ($\nu_{C\equiv N}$) in the infrared (IR) spectrum (Figure S9) corroborates the presence of the **TCNQ$^{\cdot-}$** moiety,[25,43,44] with a small shift with respect to the band for the LiTCNQ (2,203 cm^{-1}). All these characterization techniques confirm that **TCNQ$^{\cdot-}$** molecules keep their radical character in $\mathbf{1^{2+}}$**-2(TCNQ$^{\cdot-}$)**, while π interactions with the viologen should induce a small change in its electronic structure.[45]

It is noteworthy that a mixture in a 1:1 ratio also gives rise to the formation of the same complex, as a dark violet precipitate is observed. Nevertheless, after the precipitation, the solution is yellow, as an $\mathbf{1^{2+}}(Cl^-)_2$ aqueous solution, indicating that some $\mathbf{1^{2+}}(Cl^-)_2$ remains in the solution without forming the complex. This is corroborated by UV-vis spectroscopy (Figure S2), as well as by ^{1}H-NMR, as the NMR spectrum for a 1:1 ratio ($\mathbf{1^{2+}}$**-TCNQ$^{\cdot-}$**) solution shows the same peaks as those observed for a $\mathbf{1^{2+}}(Cl^-)_2$ aqueous solution (Figure S7). These results could indicate a supramolecular assembly in a 1:2 ratio ($\mathbf{1^{2+}}$**-2(TCNQ$^{\cdot-}$)**) as the predominant form, which is confirmed by single-crystal structure determination via 3D electron diffraction (see Figure 2 and the supplemental information for further details). Additionally, it is noted that a LiTCNQ aqueous solution undergoes a progressive dimerization process (Figure S3), culminating in complete dimerization after 48 h. The mixture of the

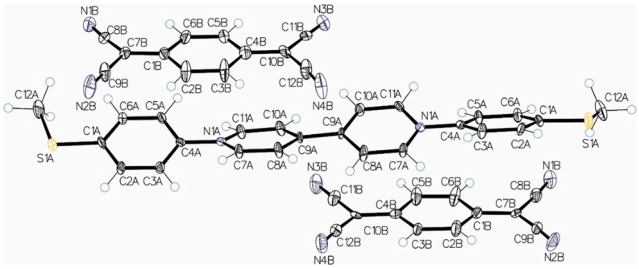

Figure 2. Crystallographic structure

Ortep drawing (thermal ellipsoids drawn at a 50% level) showing the structure of $\mathbf{1^{2+}}$**-2(TCNQ$^{\cdot-}$)** with the labeling of the atoms.

dimeric species $\mathbf{(TCNQ_2)^{2-}}$ in aqueous solution with $\mathbf{1^{2+}}(Cl^-)_2$ does not produce any significant difference in the UV-vis spectrum of the original $\mathbf{1^{2+}}(Cl^-)_2$ solution, revealing the non-formation of a supramolecular system between these two species under these conditions (Figure S4).

Supramolecular five-molecule assembly

Once the formation of the $\mathbf{1^{2+}}$**-2(TCNQ$^{\cdot-}$)** complex is proved, cucurbit[8]uril (**CB[8]**), which has been reported to form host-guest complexes with a variety of alkyl viologen derivatives with inclusion constants up to $\sim 10^6$,[12,46] is added in excess (20% more due to the presence of water in the **CB[8]**) to the $\mathbf{1^{2+}}$**-2(TCNQ$^{\cdot-}$)** once precipitation has occurred. The addition of **CB[8]** in the aqueous solution dissolves the precipitated $\mathbf{1^{2+}}$**-2(TCNQ$^{\cdot-}$)** system, resulting in a homogeneous magenta solution that remains stable over time. The UV-vis spectrum is similar to the one obtained for the $\mathbf{1^{2+}}$**-2(TCNQ$^{\cdot-}$)** solution before precipitation (Figure 1). It reveals that the supramolecular interaction of the $\mathbf{1^{2+}}$**-2(TCNQ$^{\cdot-}$)** complex is retained after the addition of **CB[8]**, and more importantly, it is consistent with inclusion within the **CB[8]** cavity. High-resolution electrospray mass spectrometry was employed to elucidate the supramolecular species formed by adding the **CB[8]** molecule. In Figure S10, two direct infusion mass spectra have been collected using two concentrations of **CB[8]**, 1:1 and 1:2, with the $\mathbf{1^{2+}}$**-2(TCNQ$^{\cdot-}$)** system. In both cases, the species detected are the same, and the systems with viologen are those that are also found in the conductance measurements: the free $\mathbf{1^{2+}}$, $\mathbf{1^{2+}}$**@CB[8]**, and, finally, the more complex species, including the five-molecule assembly, {$\mathbf{1^{2+}}$**-2(TCNQ$^{\cdot-}$)@2CB[8]**}. Also, there is a very small amount related to $\mathbf{1^{2+}}$**@2CB[8]** and an intense peak of free **CB[8]**, especially in the case of 1:2 stoichiometry. It is expected to form an assembly with two **CB[8]** molecules, as the cavity size of this host system is adequate to accommodate two stacked molecules (one **TCNQ$^{\cdot-}$** and half a $\mathbf{1^{2+}}$ viologen). This result is confirmed by density functional theory (DFT) calculations, which will be presented later. Numerous attempts to resolve the {$\mathbf{1^{2+}}$**-2(TCNQ$^{\cdot-}$)@2CB[8]**} complex by electron diffraction have shown that two types of crystals precipitate separately: $\mathbf{1^{2+}}$**-2(TCNQ$^{\cdot-}$)** and **CB[8]** crystals.

The ^{1}H-NMR spectrum for the {$\mathbf{1^{2+}}$**-2(TCNQ$^{\cdot-}$)@2CB[8]**} aqueous solution shows peaks attributed to the excess amount of **CB[8]** in solution and very low intense peaks attributed to the formation of the $\mathbf{1^{2+}}$**@CB[8]** host-guest complex (Figure S7),[12] suggesting the presence of a small amount of free $\mathbf{1^{2+}}$ in the

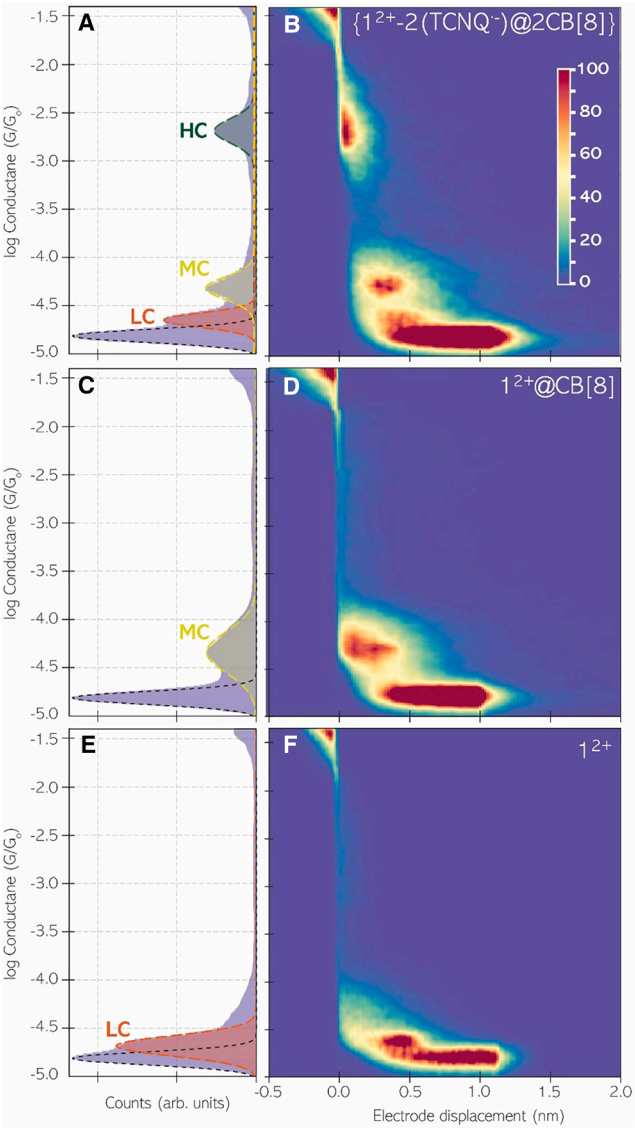

Figure 3. Electrical properties

1D conductance and 2D conductance-displacement semi-log histograms of clustered tapping datasets for the (A and B) **{1^{2+}-2(TCNQ$^{\cdot-}$)@2CB[8]}** host-guest complex and (C and D) **1^{2+}@CB[8]** and (E and F) **1^{2+}** systems, with single-molecule junctions. The green, yellow, and red dashed traces represent Gaussian fits for the high-conductance (HC), medium-conductance (MC), and low-conductance (LC) regimes, respectively. Black traces correspond to the Gaussian fitting of the background offset current.

(A and B) Histograms were built after analyzing a total of 16,386 current decays. Fitting parameters: LC (mean: −4.63, SD: 0.912, FWHM: 1.93), MC (mean: −4.28, SD: 1.113, FWHM: 2.12), and HC (mean: −2.69, SD: 1.55, FWHM: 3.03).

(C and D) Histograms built after analyzing a total of 4,581 current decays. Fitting parameters: −4.19, SD: 0.885, FWHM: 1.97. Note the consistency between these fitting parameters and those obtained for the same MC current signature present in (A).

(E and F) Histograms built after analyzing a total of 5,121 current decays. Fitting parameters: mean = −4.73, SD = 0.945, FWHM = 2.23. The scale bar represents the counts normalized, from 0 to 100, to the total number of processed captures to have equivalent ranges between sets of experiments. The applied bias voltage is set to +30 mV. For a detailed quantitative evaluation of plateau lengths, the reader is referred to the 1D histogram analysis in Figures S20–S22.

solution, while the absence of the peaks attributed to **$(TCNQ_2)^{2-}$** (Figure S7) demonstrated that all TCNQ present in the solution forms the **1^{2+}-2(TCNQ$^{\cdot-}$)** complex, as confirmed by EPR and IR spectroscopy. The IR spectrum for **{1^{2+}-2(TCNQ$^{\cdot-}$)@2CB[8]}** displays a band at 2,194 cm^{-1} attributed to the **TCNQ$^{\cdot-}$** moiety (Figure S9)[25,43,44]; meanwhile, the EPR spectrum shows a similar band to that observed for **1^{2+}-2(TCNQ$^{\cdot-}$)**, albeit with a slight shift of the *g* factor attributed to the presence of the **CB[8]** molecules (Figure S8).

Electronic properties

The electronic properties of the five-molecule **{1^{2+}-2(TCNQ$^{\cdot-}$)@2CB[8]}** host-guest complex are determined by employing the tapping[47,48] (dynamic) STM-BJ approach (Figure S15A). Briefly, in the tapping approach, the STM tip electrode is repeatedly driven into and out of contact with the substrate electrode under STM piezo servo's current-feedback-loop-off conditions.[47] During the tip electrode retraction, the current signal is monitored in real time and shows an exponential decay. When the metallic contact between the two electrodes is broken, individual molecules can make electrical contact between both electrodes and be detected as current steps or plateaus in the current decay, attesting to single-molecule junctions. Thousands of current decays are collected (as shown in Figure S16) and then clustered by using our own designed unsupervised machine learning statistical algorithm (see the supplemental information for details) to distinguish those decays with plateaus from those without plateaus. 1D semi-log conductance and 2D semi-log conductance-displacement histograms are constructed from these clustered datasets with (Figure 3) and without (Figure S23) single-molecule junctions.

Figures 3A and 3B show the 1D conductance and 2D conductance-displacement semi-log histograms of the single-molecule tapping measurements for an aqueous solution of **{1^{2+}-2(TCNQ$^{\cdot-}$)@2CB[8]}**. Three molecular conductance signatures are obtained with mean values of $10^{-2.7}$, $10^{-4.3}$, and $10^{-4.6}$ G_0 in well-differentiated regimes, which are labeled as high conductance (HC), medium conductance (MC), and low conductance (LC) and are attributed to the **{1^{2+}-2(TCNQ$^{\cdot-}$)@2CB[8]}** host-guest complex and the **1^{2+}@CB[8]** and **1^{2+}** systems, respectively (Table S9), as will be demonstrated later. All three regimes have yields (junction probability formation) of 22.3%, 14.2%, and 8.9%, respectively, over the total of the current decays (16,386 current decays without and with junctions) (see Table S10). These values are within the typical range for single-molecule current measurements, as reported in previous studies.[49–51]

According to previous studies, the observed MC and LC values are assigned to the presence of residual **1^{2+}@CB[8]** and free **1^{2+}**,[12] respectively. Nevertheless, to attest to the nature of both MC and LC molecular conductance signatures in our system, control tapping measurements of **1^{2+}@CB[8]** and **1^{2+}** are carried out. The conductance signatures obtained for both systems (Figures 3C–3F, respectively) confirm the assignment of these conductance signatures to these species, MC to **1^{2+}@CB[8]** and LC to **1^{2+}**. While 2D conductance-displacement maps provide a qualitative visualization of the trace population distribution, quantitative plateau lengths are extracted from the statistical analysis of 1D histograms (see Figures S20–S22).

The mean plateau lengths for MC and LC junctions were found to be 0.82 and 0.86 nm, respectively, once a ~0.5 nm gold snapback was added[52] (see Figures S20 and S21). These observations are consistent with those reported in earlier studies on **1^{2+}@CB[8]** and **1^{2+}**, respectively.[10,12] Therefore, the HC signature is assigned to the {**1^{2+}-2(TCNQ$^{\cdot-}$)@2CB[8]**} supramolecular host-guest complex based on the mass spectra of Figure S10. Assigning these values to the other {**1@2CB[8]**} system detected in the mass spectrometer can be discarded, as these HC values are not observed in experiments performed without TCNQ. We speculate that the increase in conductance value by almost two orders of magnitude, compared to **1^{2+}@CB[8]**, may be triggered by the intermolecular interaction between **1^{2+}** and **TCNQ$^{\cdot-}$** and its stabilization by **CB[8]**.[13,53] An increase in the molecular conductance in the same order of magnitude as that obtained here was also observed for a supramolecular complex between tetracyanoethylene (TCNE) and α-quaterthiophene in single-molecule junctions,[13] while only an enhancement in molecular conductance up to 10-fold is observed for the redox pair ($V^{2+/+}$) to the radical cationic state in the electrolytic solution of a similar viologen derivative.[15,51] Additionally, as **1^{2+}-2(TCNQ$^{\cdot-}$)** is insoluble (see Figure 1), molecular conductance histograms for this system, in a 1:1 ratio, using tapping measurements, only showed that the signature attributed to free **1^{2+}** remained in the aqueous solution once the **1^{2+}-2(TCNQ$^{\cdot-}$)** complex was precipitated (Figure S17).

The three molecular junctions' mean plateau lengths followed a negative correlation with the conductance, as HC < MC < LC. HC signatures show the shortest mean plateau length of 0.71 nm, where a ~0.5 nm gold snapback has been added (Figure S22), decreasing meaningfully from MC and LC characteristic values due to the intrinsically significantly lower resistance of the HC molecular junctions.[54,55] In them, the junction stability is reduced as a consequence of the inherent local heating resulting from more robust electron-phonon interactions[56] and due to electromigration-induced metal atom mobility. This is more pronounced in such HC levels,[56,57] as the conductance of the HC level is more than two orders of magnitude higher than that of the MC and LC levels. Previous STM break-junction studies[54] have highlighted similar effects, which can account for the differences in plateau lengths observed in our experiments.

Tapping control experiments of **CB[8]** molecules in solution with the presence of **TCNQ$^{\cdot-}$** were also performed to discard any effect of one or both combined species over the detected HC signature. In these control experiments, no conductance signals are detected (Figure S18). To ensure that **CB[8]** detection does not go unnoticed despite having molecular junctions, more robust and stable junctions over time are promoted by employing the blinking approach.[58] The blinking static approach avoids the mechanical stress commonly induced by the tapping dynamic approach, since the latter entails instabilities to the molecular junction.[54,59] Hence, **CB[8]** measurements with and without **TCNQ$^{\cdot-}$** in solution are repeated using the same blinking approach (Figure S19). Molecular junctions of $10^{-4.0}$ G_0, in agreement with previous results,[60] and an average lifetime of ca. 0.09 s (inset, Figure S19) are detected for both sets of blinking experiments. Therefore, this result excludes, on the one hand, any effect of the **TCNQ$^{\cdot-}$** over the **CB[8]** conductance in our current region of interest and, on the other hand, that the obtained conductance is due to the **CB[8]**, as attested by previous studies.[60] We attribute the short lifetimes of **CB[8]** junctions, in comparison with common anchoring groups,[54,61] to the low affinity of the O-based terminal groups for Au electrodes,[48] which reinforces the absence of the **CB[8]** current signal in the tapping measurements (Figure S18). Therefore, tapping and blinking measurements also rule out any possible relationship between **CB[8]** and **TCNQ$^{\cdot-}$**, as free molecules or combined, as the origin of the HC signatures.

Theoretical calculations

To corroborate the experimental results, a theoretical analysis divided into two parts is carried out. In the first part, the aim is to analyze the stability of the different supramolecular species that can be formed. In the second part, the transport properties through the {**1^{2+}-2(TCNQ$^{\cdot-}$)@2CB[8]**} host-guest complex are studied, and the increase in conductance for the HC case with respect to free **1^{2+}** is corroborated.

For the study of the stability of the supramolecular species, the fhi-aims computer code[62,63] is used, and all systems are optimized using the Perdew-Burke-Ernzerhof (PBE) functional,[64] adding dispersion terms using the many-body methodology,[65] and a tight numerical basis is used. The optimized geometries and calculated energy values are included as supplemental information. For the study, the sequence of experimental steps is followed as a reference. Firstly, in the reaction of **1^{2+}** with **TCNQ$^{\cdot-}$**, it is found that the formation of the neutral π-stacked **1^{2+}-2(TCNQ$^{\cdot-}$)** system is favorable in comparison with a 1:1 stoichiometry by more than 70 kcal/mol. These data confirm the experimental tendency to form such systems. Likewise, the tendency of **TCNQ$^{\cdot-}$** to form dimeric species **$(TCNQ_2)^{2-}$** is well known and has been mentioned previously. If we compare the formation energy of the alternating **TCNQ$^{\cdot-}$-1^{2+}-TCNQ$^{\cdot-}$** complex with a **1^{2+}-$(TCNQ_2)^{2-}$** complex with **TCNQ$^{\cdot-}$** maintaining the dimer structure, the alternating structure is about 11 kcal/mol more stable, in agreement with a previously described control experiment. Once this alternating complex is formed, the size **TCNQ$^{\cdot-}$-1^{2+}-TCNQ$^{\cdot-}$** is well matched to the **CB[8]** to form supramolecular assemblies. At the level of the theoretical study, we have considered both the formation of {**1^{2+}-2(TCNQ$^{\cdot-}$)@CB[8]**} with the three molecules inside **CB[8]** (Figure 4A) and the system concordant with the mass spectrometry results, {**1^{2+}-2(TCNQ$^{\cdot-}$)@2CB[8]**}, where a supramolecular complex with five molecules is formed with each **CB[8]** in each side of the **1^{2+}** including a **TCNQ$^{\cdot-}$**. The formation of the {**1^{2+}-2(TCNQ$^{\cdot-}$)@CB[8]**} system from **1^{2+}-2(TCNQ$^{\cdot-}$)** and **CB[8]** is energetically favored, −62 kcal/mol. Nevertheless, the incorporation of a second **CB[8]** (Figure 4B) is 41.7 kcal/mol more stable than {**1^{2+}-2(TCNQ$^{\cdot-}$)@CB[8]**} and a free **CB[8]**. Thus, these data corroborate the results of mass spectrometry. Additionally, an analysis of host-guest structures with **CB[8]** in the Cambridge Structural Database reveals a clear preference for having two relatively flat molecules inside rather than including three.[66]

Analysis of the **TCNQ$^{\cdot-}$-1^{2+}-TCNQ$^{\cdot-}$** unit's electronic structure indicates that there is not complete charge transfer from **TCNQ$^{\cdot-}$** to **1^{2+}** to give a complex with three neutral molecules.

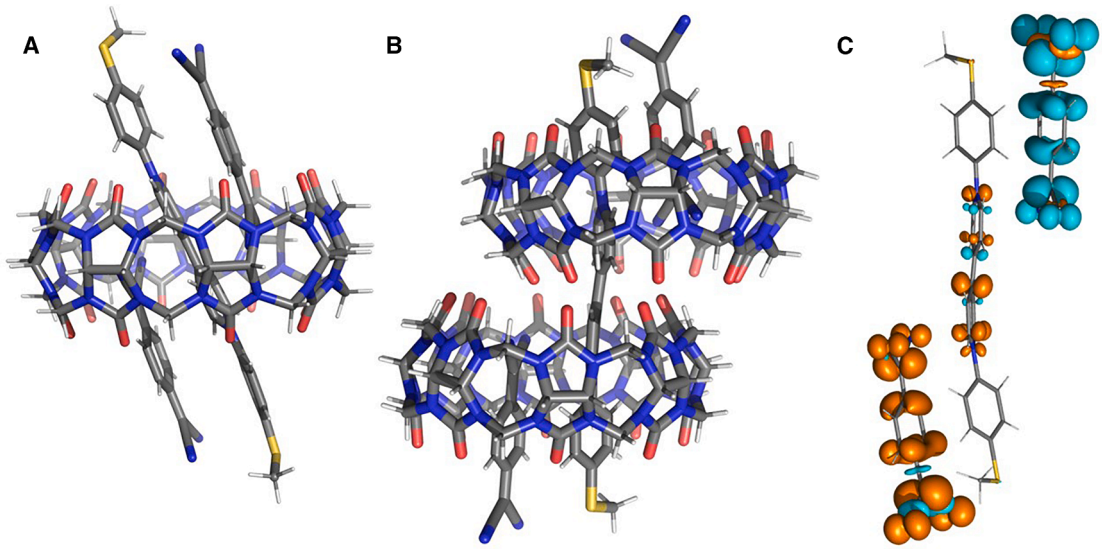

Figure 4. DFT calculations

(A and B) DFT-optimized structures (PBE functional + many-body dispersion) of (A) {$\mathbf{1^{2+}}$**-2(TCNQ$^{\cdot-}$)@CB[8]**} and (B) {$\mathbf{1^{2+}}$**-2(TCNQ$^{\cdot-}$)@2CB[8]**}.
(C) Calculated spin density of the **TCNQ$^{\cdot-}$-1^{2+}-TCNQ$^{\cdot-}$** unit with the structure in {$\mathbf{1^{2+}}$**-2(TCNQ$^{\cdot-}$)@2CB[8]**}.

The electrostatic interaction is larger and causes the charged species to be retained (in agreement with the EPR and IR spectra; Figures S8 and S9, which show that the **TCNQ$^{\cdot-}$** radical character is maintained). In addition, there is also an interaction of the π systems of the three molecules, which leads to a delocalization of the spin density on the π orbitals of $\mathbf{1^{2+}}$ (Figure 4C). The spin density in Figure 4C corresponds to the antiparallel spin alignment of the two **TCNQ$^{\cdot-}$** radicals, which, in the calculation, appears at 285 cm^{-1} and is more stable than the ferromagnetic coupling between them. This spin delocalization modifies the electronic structure of $\mathbf{1^{2+}}$ and would justify the significant change in the transport through the molecule. To this electronic effect, an important structural effect also has to be added, since the dihedral angle between the two pyridine rings of the viologen molecule goes from 46.2° to 47.8° for the optimized $\mathbf{1^{2+}}$ and {$\mathbf{1^{2+}}$**@CB[8]**} structures to 14.7° in {$\mathbf{1^{2+}}$**-2(TCNQ$^{\cdot-}$)@2CB[8]**}.

The calculation of the transport properties is performed with the same fhi-aims program using the AITRANSS module.[67–69] In this case, a *meta*-GGA r^{2}SCAN functional[70] is used, as it provides a better description of the energies of the frontier orbitals near the Fermi level than the generalized gradient approximation (GGA) functional, such as the PBE used in the calculation of the formation of supramolecular species. Additionally, corrections for relativistic scalar effects are included in this calculation using the zero-order regular approximation (ZORA) method, especially due to the presence of gold atoms, as implemented in the fhi-aims code.[71] Here, we will focus on the transport of the HC peak in the conductance histograms, in comparison with MC and LC values that were already assigned to the presence of residual $\mathbf{1^{2+}}$**@CB[8]** and free $\mathbf{1^{2+}}$, respectively.[12] In Figure 5, the transmission curves in the Fermi-level region for $\mathbf{1^{2+}}$ and the supramolecular complexes {$\mathbf{1^{2}}$**@CB[8]**} and {$\mathbf{1^{2+}}$**-2(TCNQ$^{\cdot-}$)@2CB[8]**} are shown.

These transmission values at the Fermi level confirm the experimental data, indicating an increase in the conductance of the supramolecular {$\mathbf{1^{2+}}$**-2(TCNQ$^{\cdot-}$)@2CB[8]**}complex compared to $\mathbf{1^{2+}}$ and {$\mathbf{1^{2+}}$**@CB[8]**}, with the former system exhibiting an almost perfectly resonant transport. To analyze in more detail the nature of the change in the experimental conductance values between the $\mathbf{1^{2+}}$ and {$\mathbf{1^{2+}}$**-2(TCNQ$^{\cdot-}$)@2CB[8]**} systems, two additional calculations have been performed on the {$\mathbf{1^{2+}}$**-2(TCNQ$^{\cdot-}$)@2CB[8]**} supramolecular structure. The first one removes the **CB[8]** molecules, and the second one also eliminates the **TCNQ$^{\cdot-}$** anions. The result of the calculation with only the free $\mathbf{1^{2+}}$ but with the flatter structure, as it is in the {$\mathbf{1^{2+}}$**-2(TCNQ$^{\cdot-}$)@2CB[8]**} system, only implies an increase by a factor of two in the conductance in comparison with free $\mathbf{1^{2+}}$. However, the conductance through the $\mathbf{1^{2+}}$**-2(TCNQ$^{\cdot-}$)** system is around 15 times larger than that of free $\mathbf{1^{2+}}$. Thus, such results confirm that the supramolecular interaction between $\mathbf{1^{2+}}$ and **TCNQ$^{\cdot-}$** is the key factor responsible for the significant enhancement in the conductance.

In conclusion, a high-conductance molecular electronic device has been developed using a supramolecular assembly strategy. An initial π-stacked system is formed by directly adding an aqueous solution of a viologen derivative (**1**[Cl_2]) over Li**TCNQ** powder in a 1:2 ratio, respectively. The formation of the three-molecule system is evidenced by a qualitative color change and by UV-vis spectroscopy, in agreement with similar, previously reported systems. The neutral $\mathbf{1^{2+}}$**-2(TCNQ$^{\cdot-}$)** system precipitates in water, which can be dissolved by encapsulating it into two host molecules (**CB[8]**), forming a supramolecular five-molecule assembly that provides stability in solution to the system. The electronic properties of this supramolecular complex, {$\mathbf{1^{2+}}$**-2(TCNQ$^{\cdot-}$)@2CB[8]**}, lead to an increase in the molecular junction conductance value close to two orders of magnitude in comparison with $\mathbf{1^{2+}}$. DFT calculations confirm

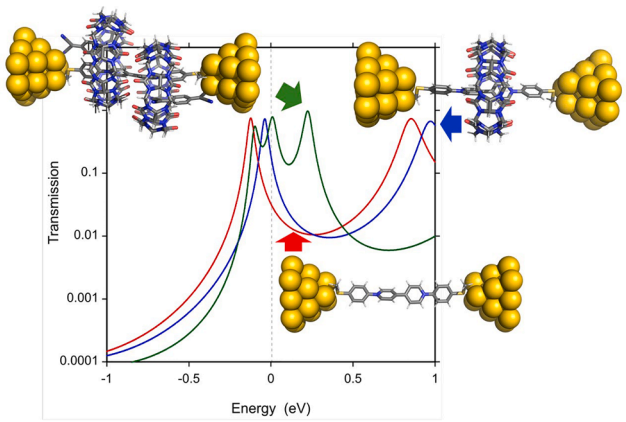

Figure 5. Transmission curves

Calculated transmission curves using fhi-aims/AITRANSS codes with the r^{2}SCAN functional for $\mathbf{1}^{2+}$ (red), {$\mathbf{1}^{2+}$**@CB[8]**} (blue), and {$\mathbf{1}^{2+}$**-2(TCNQ**$^{\cdot-}$**)@2CB[8]**} (green). The transport relationship when integrating the transmission curves using the experimental bias of 30 mV results in 1:5.8:22 for $\mathbf{1}^{2+}$, {$\mathbf{1}^{2+}$**@CB[8]**}, and {$\mathbf{1}^{2+}$**-2(TCNQ**$^{\cdot-}$**)@2CB[8]**}, respectively.

the stability of the supramolecular assembly formed and also corroborate the increase in transport through $\mathbf{1}^{2+}$ due to the interaction with **TCNQ**$^{\cdot-}$ in the formed supramolecular assembly {$\mathbf{1}^{2+}$**-2(TCNQ**$^{\cdot-}$**)@2CB[8]**}.

The fact that such enhancement of conductance is based on supramolecular interactions makes this strategy suitable for the potential fabrication of molecular electronic components with reversible states, such as molecular switches, transistors, or memory storage devices.

METHODS

Materials

1[Cl_2][12] and Li**TCNQ**[72] were synthesized according to previously published procedures. Cucurbit[8] uril hydrate (**CB8**) was purchased from Sigma-Aldrich (Merck) and used as received. To prevent the dimerization process of the LiTCNQ ($\mathbf{(TCNQ_2)^{2-}}$), a 10^{-4} M aqueous solution of **1**[Cl_2] was added directly to the Li**TCNQ** powder. **CB8** powder was added directly to the $\mathbf{1}^{2+}$**-2(TCNQ**$^{\cdot-}$**)** suspension and under sonication for 10 min. Water was purified on a Milli-Q system (resistivity: 18.2 MΩ·cm).

Characterization

UV-vis spectra of solutions were obtained with a Varian Cary 50 Bio UV-vis spectrophotometer in quartz cuvettes with an incident angle of 90°. NMR experiments were performed at 298 K on a Bruker Neo 500 spectrometer in H_2O using excitation sculpting with gradients to suppress the water signal (pulse sequence *zgesgp* from the Bruker library). TMSP-d_4 (3-(trimethylsilyl)propionic-2,2,3,3-d_4 acid sodium salt) was used as an internal reference. EPR studies were carried out in a Bruker ELEXSYS 580 spectrometer, capable of performing experiments in continuous mode in X and Q bands (around 9.5 and 34 GHz, respectively) and in pulsed mode in the X band. Attenuated total reflection IR (ATR-IR) spectra were recorded on a PerkinElmer Spectrum 100 Fourier transform infrared spectroscopy (FTIR spectroscopy) spectrometer. Electrospray mass spectra were registered in an LTQ Orbitrap Velos equipment. Single-crystal structures were obtained by using sample grains in a XtalLAB Synergy-ED from Rigaku-JEOL, provided with a HyPix-ED detector and a LiB6 200 kV electron source (200 kV, 101.20 μA) in shutterless operation mode. The wavelength was 0.0251 Å. The total dose for the five merged crystal grains was 37.125 $e^-/Å^2$, with a condenser strength of 1. Magnification diffraction: 50 cm, IL1 projection focus: hex 5301 (21245), CL 10 μm, SA 100 μm, distance (camera length): 643 mm, scan width: 0.25°, and exposure time 1.00 s/degree. Meanwhile, data processing was carried out using CrysAlis^{Pro} 44.89a (Rigaku) and structure processing using Olex2 v.1.5-ac7-014 OlexSys 2004–2024. See the supplemental methods for more details.

Electrical measurements

The electrical properties were determined by employing the tapping (dynamic) and/or blinking (static) STM-BJ approaches. See the supplemental methods for further details.

RESOURCE AVAILABILITY

Lead contact

Requests for further information and resources should be directed to and will be fulfilled by the lead contact, Santiago Martín (smartins@unizar.es).

Materials availability

This study did not generate new, unique reagents or materials.

Data and code availability

- All data reported in this paper will be made available by the lead contact upon request. Crystallography data for the structures reported in this article have been deposited at the CCDC under deposition number 2457276. Copies of the data can be obtained free of charge via https://www.ccdc.cam.ac.uk/structures/. Source data are provided with this paper.
- This paper does not report original code.
- Any additional information required to reanalyze the data reported in this paper is available from the lead contact upon request.

ACKNOWLEDGMENTS

E.E. gratefully acknowledges the award of a DGA fellowship from the government of Aragon and Campus Iberus e Erasmus-Programme, Universidad de Zaragoza; Fundación Bancaria Ibercaja; and Fundación CAI (CB 7/21) for international research stay cofunding. P.C. and S.M. are grateful for financial assistance in the framework of the project PID2022-141433OBI00 funded by MCIN/AEI/10.13039/501100011033 and by "ERDF A way of making Europe" as well as Gobierno de Aragón through grant E31_23R with European Social Funds (Construyendo Europa desde Aragón). P.R. acknowledges financial support from project PID2021-126132NB-I00 from MCIN/AEI/10.13039/501100011033 and by "ERDF A way of making Europe." We received financial support from Ministerio de Ciencia, Innovación y Universidades (PID2024-155562NB-I00, TED2021-129593B-I00, and Maria de Maeztu CEX2021-001202-M). We also acknowledge the Generalitat de Catalunya for the 2021-SGR-00286 grant, E.R. for an ICREA Academia grant, B.M. for a Beatriu de Pinós grant, and A.C.A. as a Serra Hunter Fellow. A.C.A. is grateful for generous funding through the Max Planck Society. We are thankful for the use of computational resources from the CSUC and BSC supercomputer centers. The authors would like to acknowledge the use of the SAI (Unizar), CEQMA (UNIZAR-CSIC) Services, and Laboratorio de Microscopias

Avanzadas (LMA, UNIZAR). The authors also thank Dr. Inés García for technical support in EPR studies, Dr. Andrea Vezzoli for technical support in the preliminary single-molecule conductance experiments, and Laura Ortiz for the electrospray mass spectra carried out in the CCiTUB. The ICIQ and J.B.-B., as those responsible for the electron diffractometer, thank the Ministerio de Ciencia e Innovación and the European Union NextGenerationEU for financing the Electron Diffractometer Synergy-ED with the project EQC2021-006956-P/AEI/10.13039/501100011033.

AUTHOR CONTRIBUTIONS

Conceptualization, E.E., P.C., E.R., A.C.A., and S.M.; synthesis, E.E., R.J.D., and S.M.; methodology, E.E. and M.R.A.; software, S.C. and A.C.A.; validation, E.E., M.R.A., B.M., E.R., A.C.A., and S.M.; acquisition and NMR analysis, E.E. and P.R.; formal analysis, E.E., M.R.A., S.C., E.R., A.C.A., and S.M.; investigation, E.E., M.R.A., B.M., S.M., and J.B.-B.; data curation, E.E., M.R.A., S.C., E.R., A.C.A., and S.M.; writing – original draft preparation, E.E., A.C.A., E.R., S.M., and J.B.-B.; visualization, E.E., M.R.A., S.C., P.C., E.R., A.C.A., S.M., and J.B.-B.; supervision, E.R., A.C.A., and S.M.; funding acquisition, P.C., E.R., A.C.A., and S.M.; writing – review & editing, all authors. All authors have given approval to the final version of the manuscript.

DECLARATION OF INTERESTS

The authors declare no conflicts of interest.

SUPPLEMENTAL INFORMATION

Supplemental information can be found online at https://doi.org/10.1016/j.xcrp.2025.103029.

Received: July 10, 2025
Revised: October 2, 2025
Accepted: November 21, 2025
Published: December 18, 2025

REFERENCES

1. Li, T., Bandari, V.K., and Schmidt, O.G. (2023). Molecular Electronics: Creating and Bridging Molecular Junctions and Promoting Its Commercialization. Adv. Mater. *35*, 2209088.
2. Zhao, Y., Liu, W., Zhao, J., Wang, Y., Zheng, J., Liu, J., Hong, W., and Tian, Z.Q. (2022). The fabrication, characterization and functionalization in molecular electronics. Int. J. Extrem. Manuf. *4*, 022003.
3. Marqués-González, S., and Low, P.J. (2016). Aust. J. Chem. *69*, 244–253.
4. Su, T.A., Neupane, M., Steigerwald, M.L., Venkataraman, L., and Nuckolls, C. (2016). Chemical principles of single-molecule electronics. Nat. Rev. Mater. *1*, 16002.
5. Tang, C., Ayinla, R.T., and Wang, K. (2022). Beyond electrical conductance: progress and prospects in single-molecule junctions. J. Mater. Chem. C *10*, 13717–13733.
6. Bei, Z., Huang, Y., Chen, Y., Cao, Y., and Li, J. (2020). Photo-induced carbocation-enhanced charge transport in single-molecule junctions. Chem. Sci. *11*, 6026–6030.
7. Fatemi, V., Kamenetska, M., Neaton, J.B., and Venkataraman, L. (2011). Environmental Control of Single-Molecule Junction Transport. Nano Lett. *11*, 1988–1992.
8. Wu, C., Qiao, X., Robertson, C.M., Higgins, S.J., Cai, C., Nichols, R.J., and Vezzoli, A. (2020). A Chemically Soldered Polyoxometalate Single-Molecule Transistor. Angew. Chem. Int. Ed. *59*, 12029–12034.
9. Song, H., Kim, Y., Jang, Y.H., Jeong, H., Reed, M.A., and Lee, T. (2009). Observation of molecular orbital gating. Nature *462*, 1039–1043.
10. Yu, H., Li, J., Li, S., Liu, Y., Jackson, N.E., Moore, J.S., and Schroeder, C.M. (2022). Efficient Intermolecular Charge Transport in π-Stacked Pyridinium Dimers Using Cucurbit[8]uril Supramolecular Complexes. J. Am. Chem. Soc. *144*, 3162–3173.
11. Nishino, T., Hayashi, N., and Bui, P.T. (2013). Direct Measurement of Electron Transfer through a Hydrogen Bond between Single Molecules. J. Am. Chem. Soc. *135*, 4592–4595.
12. Zhang, W., Gan, S., Vezzoli, A., Davidson, R.J., Milan, D.C., Luzyanin, K.V., Higgins, S.J., Nichols, R.J., Beeby, A., Low, P.J., et al. (2016). Single-Molecule Conductance of Viologen–Cucurbit[8]uril Host–Guest Complexes. ACS Nano *10*, 5212–5220.
13. Wang, K., Vezzoli, A., Grace, I.M., McLaughlin, M., Nichols, R.J., Xu, B., Lambert, C.J., and Higgins, S.J. (2019). Charge transfer complexation boosts molecular conductance through Fermi level pinning. Chem. Sci. *10*, 2396–2403.
14. Almughathawi, R., Hou, S., Wu, Q., Liu, Z., Hong, W., and Lambert, C. (2021). Conformation and Quantum-Interference-Enhanced Thermoelectric Properties of Diphenyl Diketopyrrolopyrrole Derivatives. ACS Sens. *6*, 470–476.
15. Li, J., Pudar, S., Yu, H., Li, S., Moore, J.S., Rodríguez-López, J., Jackson, N.E., and Schroeder, C.M. (2021). Reversible Switching of Molecular Conductance in Viologens is Controlled by the Electrochemical Environment. J. Phys. Chem. C *125*, 21862–21872.
16. Ayinla, R.T., Shiri, M., Song, B., Gangishetty, M., and Wang, K. (2023). The pivotal role of non-covalent interactions in single-molecule charge transport. Mater. Chem. Front. *7*, 3524–3542.
17. Hunter, C.A. (1994). Meldola Lecture. The role of aromatic interactions in molecular recognition. Chem. Soc. Rev. *23*, 101–109.
18. Pérez, E.M., Capodilupo, A.L., Fernández, G., Sánchez, L., Viruela, P.M., Viruela, R., Ortí, E., Bietti, M., and Martín, N. (2008). Chem. Commun., 4567–4569.
19. Neel, A.J., Hilton, M.J., Sigman, M.S., and Toste, F.D. (2017). Exploiting non-covalent π interactions for catalyst design. Nature *543*, 637–646.
20. Proctor, R.S.J., Colgan, A.C., and Phipps, R.J. (2020). Exploiting attractive non-covalent interactions for the enantioselective catalysis of reactions involving radical intermediates. Nat. Chem. *12*, 990–1004.
21. Rest, C., Kandanelli, R., and Fernández, G. (2015). Chem. Soc. Rev. *44*, 2573.
22. Song, S., Wang, L., Su, J., Xu, Z., Hsu, C.H., Hua, C., Lyu, P., Li, J., Peng, X., Kojima, T., et al. (2021). Manifold dynamic non-covalent interactions for steering molecular assembly and cyclization. Chem. Sci. *12*, 11659–11667.
23. Xu, Y., Hao, J., Ju, H., He, S., Wang, J., Jia, C., and Guo, X. (2024). Identifying π–π and π–Lone Pair Interactions in a Single-Molecule Junction. ACS Mater. Lett. *6*, 1961–1967.
24. Wang, W., Luo, L., Sheng, P., Zhang, J., and Zhang, Q. (2021). Multifunctional Features of Organic Charge-Transfer Complexes: Advances and Perspectives. Chem. Eur J. *27*, 464–490.
25. Jono, R., Fujisawa, J.i., Segawa, H., and Yamashita, K. (2011). Theoretical Study of the Surface Complex between TiO_2 and TCNQ Showing Interfacial Charge-Transfer Transitions. J. Phys. Chem. Lett. *2*, 1167–1170.
26. Chen, H.L., and Stoddart, J.F. (2021). Nat. Rev. Mater. *6*, 804–828.
27. Li, X., Ge, W., Guo, S., Bai, J., and Hong, W. (2023). Characterization and Application of Supramolecular Junctions. Angew. Chem. Int. Ed. *62*, e202216819.
28. Kim, D.S., and Sessler, J.L. (2015). Calix[4]pyrroles: versatile molecular containers with ion transport, recognition, and molecular switching functions. Chem. Soc. Rev. *44*, 532–546.
29. Molina, P., Zapata, F., and Caballero, A. (2017). Anion Recognition Strategies Based on Combined Noncovalent Interactions. Chem. Rev. *117*, 9907–9972.
30. Ward, M.D., Hunter, C.A., and Williams, N.H. (2018). Coordination Cages Based on Bis(pyrazolylpyridine) Ligands: Structures, Dynamic Behavior, Guest Binding, and Catalysis. Acc. Chem. Res. *51*, 2073–2082.

31. Webber, M.J., and Langer, R. (2017). Drug delivery by supramolecular design. Chem. Soc. Rev. *46*, 6600–6620.

32. Kassem, S., van Leeuwen, T., Lubbe, A.S., Wilson, M.R., Feringa, B.L., and Leigh, D.A. (2017). Artificial molecular motors. Chem. Soc. Rev. *46*, 2592–2621.

33. Escorihuela, E., del Barrio, J., Davidson, R.J., Beeby, A., Low, P.J., Prez-Murano, F., Cea, P., and Martin, S. (2024). Large area arrays of discrete single-molecule junctions derived from host–guest complexes. Nanoscale *16*, 1238–1246.

34. Herrer, L., Naghibi, S., Marin, I., Ward, J.S., Bonastre, J.M., Higgins, S.J., Martin, S., Vezzoli, A., Nichols, R.J., Serrano, J.L., and Cea, P. (2023). Adv. Mater. Interf. *10*, 2300133.

35. Kiguchi, M., Nakashima, S., Tada, T., Watanabe, S., Tsuda, S., Tsuji, Y., and Terao, J. (2012). Single-Molecule Conductance of π-Conjugated Rotaxane: New Method for Measuring Stipulated Electric Conductance of π-Conjugated Molecular Wire Using STM Break Junction. Small *8*, 726–730.

36. Tang, J.H., Li, Y.Q., Wu, Q.Q., Wang, Z.X., Hou, S.J., Tang, K., Sun, Y., Wang, H., Wang, H., Lu, C., et al. (2019). Nat. Commun. *10*, 4559.

37. Jiang, M., Li, S., Zhen, C., Wang, L., Li, F., Zhang, Y., Dong, W., Zhang, X., and Hu, W. (2022). Front. Optoelectron. *15*, 26.

38. Bennett, T.H., Pamu, R., Yang, G., Mukherjee, D., and Khomami, B. (2020). A new platform for development of photosystem I based thin films with superior photocurrent: TCNQ charge transfer salts derived from ZIF-8. Nanoscale Adv. *2*, 5171–5180.

39. Odom, S.A., Caruso, M.M., Finke, A.D., Prokup, A.M., Ritchey, J.A., Leonard, J.H., White, S.R., Sottos, N.R., and Moore, J.S. (2010). Restoration of Conductivity with TTF-TCNQ Charge-Transfer Salts. Adv. Funct. Mater. *20*, 1721–1727.

40. van de Wouw, H.L., Chamorro, J., Quintero, M., and Klausen, R.S. (2015). Opposites Attract: Organic Charge Transfer Salts. J. Chem. Educ. *92*, 2134–2139.

41. Mukherjee, B., and Mukherjee, M. (2011). High Performance Organic Thin Film Transistors with Solution Processed TTF-TCNQ Charge Transfer Salt as Electrodes. Langmuir *27*, 11246–11250.

42. Knowles, K.E., Malicki, M., Parameswaran, R., Cass, L.C., and Weiss, E.A. (2013). Spontaneous Multielectron Transfer from the Surfaces of PbS Quantum Dots to Tetracyanoquinodimethane. J. Am. Chem. Soc. *135*, 7264–7271.

43. Sutton, A.L., Abrahams, B.F., D'Alessandro, D.M., Hudson, T.A., Robson, R., and Usov, P.M. (2016). CrystEngComm *18*, 8906–8914.

44. Hoshyargar, F., and O'Mullane, A.P. (2016). ChemCatChem *8*, 2335–2339.

45. Goetz, K.P., Vermeulen, D., Payne, M.E., Kloc, C., McNeil, L.E., and Jurchescu, O.D. (2014). Charge-transfer complexes: new perspectives on an old class of compounds. J. Mater. Chem. C *2*, 3065–3076.

46. Bush, M.E., Bouley, N.D., and Urbach, A.R. (2005). Charge-Mediated Recognition of N-Terminal Tryptophan in Aqueous Solution by a Synthetic Host. J. Am. Chem. Soc. *127*, 14511–14517.

47. Xu, B., and Tao, N.J. (2003). Measurement of Single-Molecule Resistance by Repeated Formation of Molecular Junctions. Science *301*, 1221–1223.

48. Aragonès, A.C., Aravena, D., Cerdá, J.I., Acís-Castillo, Z., Li, H.P., Real, J.A., Sanz, F., Hihath, J., Ruiz, E., and Díez-Pérez, I. (2016). Nano Lett. *16*, 218–226.

49. Haiss, W., van Zalinge, H., Higgins, S.J., Bethell, D., Höbenreich, H., Schiffrin, D.J., and Nichols, R.J. (2003). Redox State Dependence of Single Molecule Conductivity. J. Am. Chem. Soc. *125*, 15294–15295.

50. Aragonès, A.C., Darwish, N., Saletra, W.J., Pérez-García, L., Sanz, F., Puigmartí-Luis, J., Amabilino, D.B., and Díez-Pérez, I. (2014). Nano Lett. *14*, 4751–4756.

51. Osorio, H.M., Catarelli, S., Cea, P., Gluyas, J.B.G., Hartl, F., Higgins, S.J., Leary, E., Low, P.J., Martín, S., Nichols, R.J., et al. (2015). Electrochemical Single-Molecule Transistors with Optimized Gate Coupling. J. Am. Chem. Soc. *137*, 14319–14328.

52. Huang, C., Rudnev, A.V., Hong, W., and Wandlowski, T. (2015). Break junction under electrochemical gating: testbed for single-molecule electronics. Chem. Soc. Rev. *44*, 889–901.

53. García, R., Herranz, M.A., Leary, E., González, M.T., Bollinger, G.R., Bürkle, M., Zotti, L.A., Asai, Y., Pauly, F., Cuevas, J.C., et al. (2015). Beilstein J. Org. Chem. *11*, 1068–1078.

54. Quintans, C.S., Andrienko, D., Domke, K.F., Aravena, D., Koo, S., Díez-Pérez, I., and Aragonès, A.C. (2021). Tuning Single-Molecule Conductance by Controlled Electric Field-Induced trans-to-cis Isomerisation. Appl. Sci. *11*, 3317.

55. Aragonès, A.C., and Domke, K.F. (2021). Cell Rep. Phys. Sci. *2*, 100389.

56. Huang, Z.F., Chen, F., D'Agosta, R., Bennett, P.A., Di Ventra, M., and Tao, N.J. (2007). Nature Nanotechnol *2*, 698–703.

57. Huang, Z.F., Xu, B.Q., Chen, Y.C., Ventra, M.D., and Tao, N.J. (2006). Measurement of Current-Induced Local Heating in a Single Molecule Junction. Nano Lett. *6*, 1240–1244.

58. Aragonès, A.C., Aravena, D., Valverde-Muñoz, F.J., Real, J.A., Sanz, F., Díez-Pérez, I., and Ruiz, E. (2017). J. Am. Chem. Soc. *139*, 5768–5778.

59. Inatomi, J., Fujii, S., Marqués-González, S., Masai, H., Tsuji, Y., Terao, J., and Kiguchi, M. (2015). J. Phys. Chem. C *119*, 19452–19457.

60. Wang, Y.H., Zhou, Y.F., Tong, L., Huang, H., Zheng, J.F., Xie, W., Chen, J.Z., Shao, Y., and Zhou, X.S. (2021). Revealing Supramolecular Interactions and Electron Transport in Single Molecular Junctions of Cucurbit[*n*]uril. Adv. Electron. Mater. *7*, 2100399.

61. Pla-Vilanova, P., Aragonès, A.C., Ciampi, S., Sanz, F., Darwish, N., and Diez-Perez, I. (2015). Nanotechnology *26*, 381001.

62. Blum, V., Gehrke, R., Hanke, F., Havu, P., Havu, V., Ren, X., Reuter, K., and Scheffler, M. (2009). Ab initio molecular simulations with numeric atom-centered orbitals. Comput. Phys. Commun. *180*, 2175–2196.

63. Levchenko, S.V., Ren, X., Wieferink, J., Johanni, R., Rinke, P., Blum, V., and Scheffler, M. (2015). Hybrid functionals for large periodic systems in an all-electron, numeric atom-centered basis framework. Comput. Phys. Commun. *192*, 60–69.

64. Perdew, J.P., Burke, K., and Ernzerhof, M. (1996). Generalized Gradient Approximation Made Simple. Phys. Rev. Lett. *77*, 3865–3868.

65. Tkatchenko, A., DiStasio, R.A., Car, R., and Scheffler, M. (2012). Accurate and efficient method for many-body van der Waals interactions. Phys. Rev. Lett. *108*, 236402.

66. Groom, C.R., Bruno, I.J., Lightfoot, M.P., and Ward, S.C. (2016). The Cambridge Structural Database. Acta Crystallogr. B *72*, 171–179.

67. Arnold, A., Weigend, F., and Evers, F. (2007). Quantum chemistry calculations for molecules coupled to reservoirs: formalism, implementation, and application to benzenedithiol. J. Chem. Phys. *126*, 174101.

68. Bagrets, A. (2013). Spin-Polarized Electron Transport Across Metal-Organic Molecules: A Density Functional Theory Approach. J. Chem. Theory Comput. *9*, 2801–2815.

69. Wilhelm, J., Walz, M., Stendel, M., Bagrets, A., and Evers, F. (2013). Ab initio simulations of scanning-tunneling-microscope images with embedding techniques and application to C58-dimers on Au(111). Phys. Chem. Chem. Phys. *15*, 6684–6690.

70. Furness, J.W., Kaplan, A.D., Ning, J., Perdew, J.P., and Sun, J. (2020). Accurate and Numerically Efficient r^2SCAN Meta-Generalized Gradient Approximation. J. Phys. Chem. Lett. *11*, 8208–8215.

71. Huhn, W.P., and Blum, V. (2017). One-hundred-three compound band-structure benchmark of post-self-consistent spin-orbit coupling treatments in density functional theory. Phys. Rev. Mater. *1*, 033803.

72. Cea, P., Martín, S., Villares, A., Möbius, D., and López, M.C. (2006). J. Phys. Chem. B *110*, 963–970.